

Anisotropic excitonic effects in the energy loss function of hexagonal boron nitride

S. Galambosi,¹ L. Wirtz,² J. A. Soininen,¹ J. Serrano,³ A. Marini,⁴
K. Watanabe,⁵ T. Taniguchi,⁵ S. Huotari,⁶ A. Rubio,⁷ and K. Hämäläinen¹

¹*Department of Physics, POB 64, FI-00014 University of Helsinki, Finland*

²*IEMN, CNRS UMR 8520, Dept. ISEN,*

B.P. 60069, 59652 Villeneuve d'Ascq, France

³*ICREA-Departamento de Fisica Aplicada,*

Universitat Politecnica de Catalunya, EPSC,

Av. Esteve Terradas 15, 08860 Castelldefels, Spain

⁴*CNISM, Dipartimento di Fisica, Università di Roma Tor Vergata,
via della Ricerca Scientifica, 00133 Roma, Italy*

⁵*National Institute for Materials Science,*

1-1 Namiki, Tsukuba, 305-0044, Japan

⁶*European Synchrotron Radiation Facility,*

BP 220, F-38043 Grenoble cedex, France

⁷*Nano-Bio Spectroscopy Group, ETSF Scientific Development Centre,
Universidad del País Vasco, CFM-CSIC-UPV/EHU-MPC and DIPC,*

Av. Tolosa 72, E-20018 San Sebastian, Spain

(Dated: May 7, 2010)

Abstract

We demonstrate that the valence energy-loss function of hexagonal boron nitride (*h*BN) displays a strong anisotropy in shape, excitation energy and dispersion for momentum transfer \mathbf{q} parallel or perpendicular to the *h*BN layers. This is manifested by e.g. an energy shift of 0.7 eV that cannot be captured by single-particle approaches and is a demonstration of a strong anisotropy in the two-body electron-hole interaction. Furthermore, for in-plane directions of \mathbf{q} we observe a splitting of the π -plasmon in the Γ M direction that is absent in the Γ K direction and this can be traced back to band-structure effects.

Layered hexagonal boron nitride (*h*BN) is the III-V compound counterpart of graphite. The recent interest in *h*BN is partly due to Watanabe et al. [1] who showed that *h*BN exhibits the potential for lasing at high energies (5.8 eV). This makes *h*BN an attractive candidate for optoelectronic applications in the ultraviolet energy range. Furthermore, a single layer of *h*BN is isoelectronic to graphene and can be considered the precursor material for boron nitride nanotubes. Despite the relatively simple crystal structure, *h*BN appears to be a challenge to both experiments and theory. The band-structure of *h*BN displays an indirect gap [2, 3] and the optical absorption spectrum is dominated by correlation effects leading to a strong Frenkel-type excitonic peak at 5.8 eV [3–5] in agreement with the experimental findings [1]. The origin of the fine structure of the absorption and luminescence spectra around this peak, however, is still under debate [6–8]. Recent luminescence experiments point towards the role of defects [9–11] in agreement with the theoretical suggestion in ref. 6.

A major source of experimental difficulties lies in the growth of large defect-free *h*BN crystals. This is especially important for the electronic properties since *h*BN stacking order can have a substantial effect on the band structure [12, 13]. In the case of cubic boron nitride, the discrepancies between experimental and theoretical results can often be traced back to the use of low quality samples [14].

In order to study the dynamics (e.g. possible dispersion) of the valence excitations one needs to use inelastic scattering probes such as electron energy loss spectroscopy (EELS) or non-resonant inelastic x-ray scattering (NRIXS). NRIXS has the advantage to study the dispersion of low lying excitations beyond the first Brillouin zone (1st BZ). This has been used numerous times in the past (see e.g. [15, 16]) and gives new important information on the properties of excitations at sub-unit-cell length scales [17]. When studying longitudinal excitations one often finds non-parabolic dispersions [18] and periodicity for low energy plasmons [19, 20]. The valence bands and the lowest conduction bands of *h*BN can be understood as combinations of the σ and π states of the hexagonal boron nitride sheet. At low momentum transfer the low-energy-transfer structures of the loss function can be divided into transitions between states with same parity (σ - σ^* , π - π^*) when the momentum transfer is in the plane and different parity (π - σ^* , σ - π^*) for momentum transfer along the c-axis [21]. The strong anisotropy in the electronic response can also be seen in the difference for the dielectric constants ϵ_∞ parallel and perpendicular to the planes (4.40 and

2.53, respectively [3]).

In this work, we study the loss function of *h*BN using NRIXS. We show detailed experimental results of the dispersion of various features and plasmons for the momentum transfer \mathbf{q} in different crystallographic directions within and beyond the 1st BZ. The loss features show a strong directional dependence not only in the comparison in-plane/out-of-plane but also for the different directions within the plane. The origin of the different spectral features and their direction and momentum dependence are analyzed by *ab-initio* calculations at the level of the random-phase approximation (RPA) and with methods of many-body perturbation theory. In order to exclude a perturbation of our results by the low crystal quality, we have characterized the sample in detail.

The sample was a colorless and transparent hexagonal single crystal *h*BN platelet about 700 μm wide and 70 μm thick. The ΓA direction was found to be very nearly parallel to the normal of the platelet. We used single-crystal X-ray diffraction to verify that the sample exhibited an AB-type stacking, thus ruling out other stable or metastable stacking sequences [12, 13].

The NRIXS spectra were measured on ID16 at the European Synchrotron Radiation Facility, Grenoble, France. The experiment was carried out using the eV-resolution spectrometer [22, 23]. An energy resolution of 0.6 eV was determined from the FWHM of the quasi-elastic line. The measurements were performed using the inverse scan technique [24]. The momentum transfer resolution was $\Delta q/q \approx 0.17$ near the K point.

Theoretical NRIXS spectra have been calculated at the level of the random-phase approximation (RPA) starting with the Kohn-Sham DFT wave-functions in the local-density approximation (LDA) [25]. The dielectric function is obtained through $\epsilon_{\mathbf{G},\mathbf{G}'}(\tilde{\mathbf{q}},\omega) = 1 - v(\tilde{\mathbf{q}} + \mathbf{G})\chi_{\mathbf{G},\mathbf{G}'}^0(\tilde{\mathbf{q}},\omega)$, where $v(\tilde{\mathbf{q}}) = 4\pi/|\tilde{\mathbf{q}}|^2$ is the Coulomb potential in reciprocal space and $\chi_{\mathbf{G},\mathbf{G}'}^0(\tilde{\mathbf{q}},\omega)$ is the independent particle polarizability which is obtained from a sum over transitions from occupied to unoccupied bands [26]. \mathbf{G}, \mathbf{G}' denote reciprocal lattice vectors, and $\tilde{\mathbf{q}}$ is restricted to the 1st BZ.

The loss function $\sigma(\mathbf{q},\omega)$ is then obtained from the inverse of the dielectric matrix

$$\sigma(\tilde{\mathbf{q}} + \mathbf{G},\omega) = -\text{Im}(\epsilon_{\mathbf{G},\mathbf{G}}^{-1}(\tilde{\mathbf{q}},\omega)), \quad (1)$$

where $\mathbf{q} = \tilde{\mathbf{q}} + \mathbf{G}$. Crystal local-field effects are automatically included by taking into account the off-diagonal elements of $\epsilon_{\mathbf{G},\mathbf{G}'}$ in the matrix inversion [27]. In order to compare with the

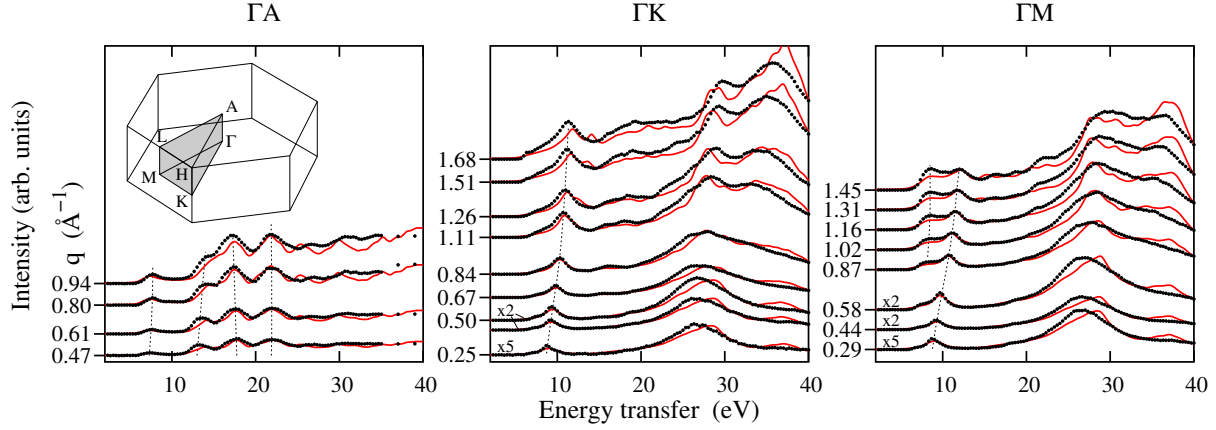


FIG. 1: (Color online) The experimental (black dots) and theoretical (red lines) NRIXS spectra in the 1st BZ along three crystallographic directions. The q^2 -weighed spectra are vertically displaced proportionally to the value of momentum transfer, which is indicated on the vertical axis. The dashed lines are guides for the eye for features discussed in the text. The inset shows the 1st BZ of $h\text{BN}$ with the irreducible part shaded.

experimental loss function, we have used a broadening $\eta = 0.4$ eV. In silicon the use of the time-dependent LDA kernel leads to a considerable enhancement in the description of short-range exchange-correlation effects [28] and to a better agreement with the experiments. We have checked that the use of time-dependent LDA does not give a substantial improvement in the case of $h\text{BN}$.

The experimental and theoretical NRIXS spectra along the three crystallographic directions within the first are depicted in Fig. 1. The experimental spectra were normalized to have the same area as the calculated spectra in the energy range shown in the figure. Overall the calculations reproduce the experimental spectra well. The *ab-initio* calculations match the experimental feature positions, their relative weights as well as the momentum transfer dependence. From the figure it is evident that the spectral features along the ΓA direction do not exhibit any significant dispersion. The high anisotropy of $h\text{BN}$ is clearly reflected in the differences between the spectra in the hexagonal plane (ΓK , ΓM) and the spectrum perpendicular to it (ΓA). For $q \lesssim 0.6 \text{ \AA}^{-1}$, the spectra along ΓK and ΓM are nearly identical. However, as the value of q is increased an anisotropy also within the hexagonal plane is clearly observed. In the high-energy range this anisotropy shows up mainly as a

different rate of relative spectral weight increase for the feature between 35 eV-40 eV. The in-plane anisotropy is most evident in the behavior of the π plasmon. Its energy disperses from 9 eV at small values of momentum transfer to about 12 eV when q is near the boundary of the 1st BZ. Along ΓM an additional peak around 8 eV develops for $q > 0.87 \text{ \AA}^{-1}$ while in the ΓK direction only a weak shoulder is detected. The double-peak structure along ΓM is also visible in $\text{Im}(\epsilon(\mathbf{q}))$. This indicates that the directional anisotropy can be interpreted in terms of interband transitions. Fig. 2 (a) shows the band structure of hBN . For $\mathbf{q} = \Gamma K$, the transitions that dominate the plasmon at 12 eV are the ones from the π band at A/H to the π^* band at H/A, respectively (red arrows). For $\mathbf{q} = \Gamma M$, the dominant transitions are the ones from the π band at A/L to the π^* band at L/A (blue arrows). The observed 8 eV transition at $\mathbf{q} = \Gamma M$ originates from a $\pi - \pi^*$ interband transition from L to a neighboring high symmetry point L'. This is marked by the vertical green arrow in Fig. 2 (a) even though it is not a vertical transition but one with a momentum difference of $\mathbf{q} = \Gamma M$. At $\mathbf{q} = \Gamma K$ the plasmon peak around 8 eV is missing because the joint-density of states displays only a minor peak there.

The ΓM and ΓK theoretical spectra have been blueshifted by 0.8 eV whereas for the ΓA spectra a blueshift of 1.5 eV was used. These shifts reflect the well-known fact that the DFT band-structure usually underestimates the transition energies between occupied and unoccupied bands. For hBN it was shown [2, 3, 6] that electron-electron correlation (calculated on the level of the GW-approximation) increases the transition energies by about 2 eV with respect to DFT-LDA calculations. At the same time, the attractive electron-hole interaction reduces the transition energy such that the difference between experimental and theoretical NRIXS spectra is less than 2 eV. We note that the GW-correction alone cannot explain the observed anisotropic shift since π and σ bands are renormalized in the same way. Therefore the experimental NRIXS data cannot be explained with single particle theories and the explicit inclusion of electron-hole interaction is necessary.

In order to check if the combined effect of electron-electron and electron-hole interaction does indeed explain the (anisotropic) shift of the RPA-spectra, we carried out calculations at selected momentum transfers including excitonic effects on the level of the Bethe-Salpeter Equation (BSE) [29]. We used the approach of Refs. [18, 30] and converged all the relevant parameters [31]. To approximate the quasi-particle band energies of Ref. 6, we used a “scissor” of 1.92 eV to shift the LDA conduction bands energies and a small stretch of 5%

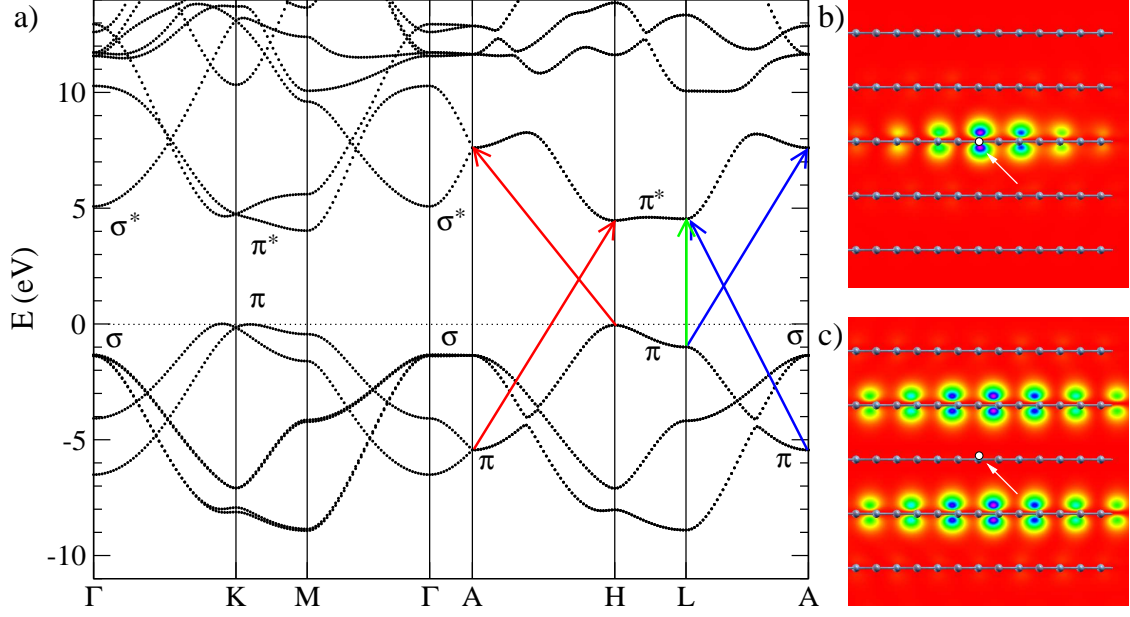


FIG. 2: (Color online) a) DFT-LDA band-structure of *h*BN. On the right the 2D projections of the electron probability density $|\Psi^\lambda(r_h, r_e)|^2$ for the lowest bright exciton in the optical absorption spectrum are shown with $\mathbf{q} \rightarrow 0$ b) parallel and c) perpendicular to the *h*BN planes. The hole position r_h (marked by white circle and arrow) is fixed 0.4 a.u. above a nitrogen atom. Balls and sticks indicate the atomic layers. Calculations of the excitonic wave functions have been performed using BSE.

was applied to the valence bands. As shown in Fig. 3 the BSE results without additional energy shifts agree well with the RPA spectra that were blueshifted to the experimental energy scale. The slight differences between the two calculations seem to originate mainly from different weights of various spectral features. Also, it should be noted, that (except for the energy shift) no extra features seem to arise in the BSE results in comparison with the RPA calculations. This confirms that the RPA successfully describes long-range excitations even in strongly anisotropic and layered materials like *h*BN, with the BSE leading only to minor corrections. Electron-hole effects can alter extended excitations only when the attraction is very strong, like in a wide-gap insulators such as LiF [29].

We found that the layered structure of *h*BN leads to a strongly anisotropic electron-hole interaction. This is demonstrated in Fig. 2 b) and c) where we show the excitonic “wave functions” for the lowest visible excitations in the optical absorption spectrum. For q parallel to the planes (q_{\parallel}), electron and hole are localized within one plane forming a strongly bound

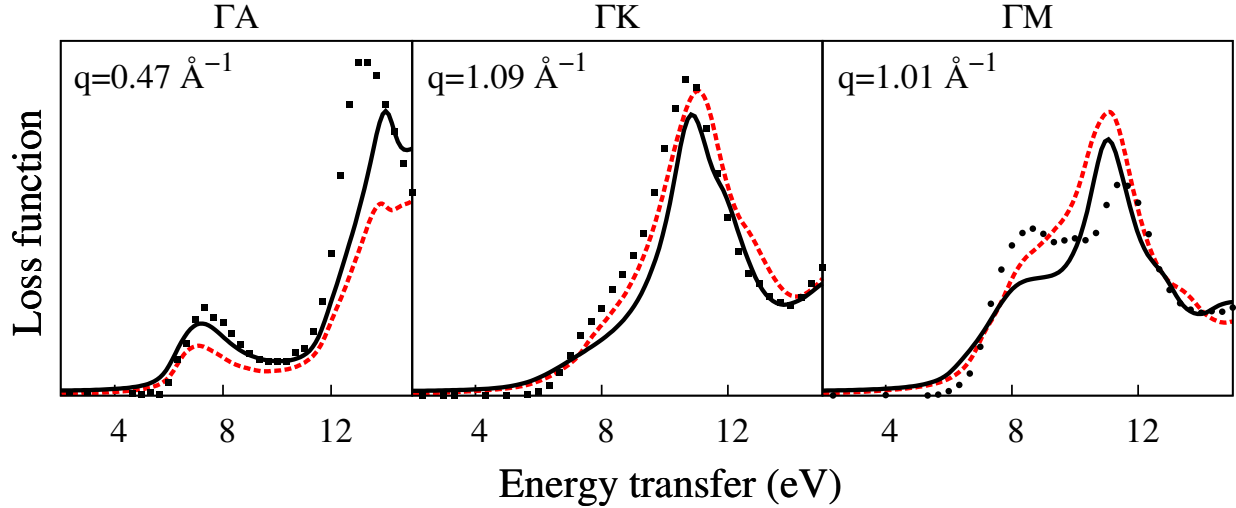


FIG. 3: (Color online) The comparison of the current RPA calculations (black solid curve) with a BSE calculation (red dashed curve) at selected momentum transfers. The RPA spectra are blueshifted as discussed in the text. Experimental data is also shown (black dots).

quasi-two dimensional compound [3, 6]. For q perpendicular (q_{\perp}), electron and hole are localized on different layers and form a more weakly bound three-dimensional compound. This leads to a larger exciton binding energy for q_{\parallel} than for q_{\perp} and thus explains why the upshift due to the combined e-e and e-h interaction is lower for q_{\parallel} than for q_{\perp} .

The NRIXS spectra with a larger range of momentum transfers directed along ΓK are displayed in Fig. 4. For most parts the calculated spectra agree well with the experimental ones. The prominent peak dispersing between 25-30 eV in the experimental spectra is reproduced very well by the calculations throughout the measured range of momentum transfers. At high momentum transfer ($> 2 \text{ \AA}^{-1}$) a new peak showing a small dispersion appears just above 20 eV. Its appearance and dispersion is reproduced well by the calculation. In the same momentum transfer range calculation shows a peak at around 15 eV which in the experiments appears to be less well pronounced and at a few eVs higher in energy. Around 7 eV in the high momentum transfer experimental spectra a sharp peak is observed, which is not present in the calculated spectra.

In conclusion, we have studied the anisotropy in the valence electron dynamics of hBN using NRIXS. Besides the in-plane/out-of-plane anisotropy, the in-plane spectra show a directional dependence at large q . In particular, the π -plasmon is split along the high

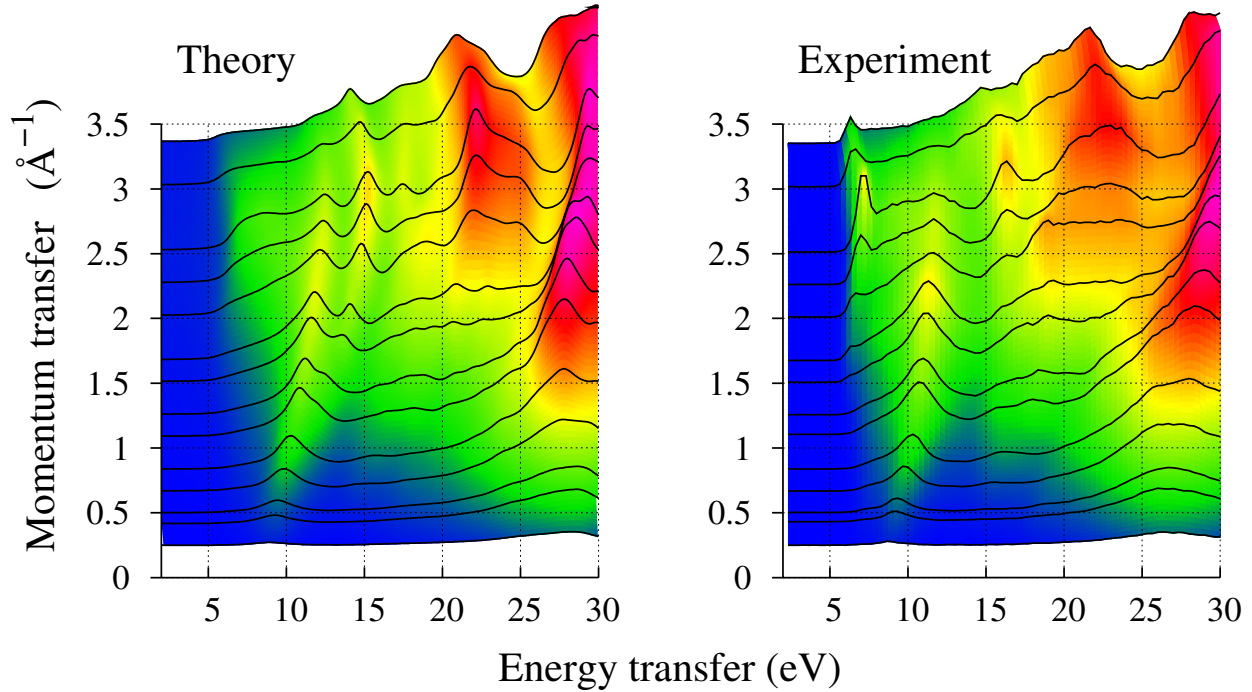


FIG. 4: (Color online) The theoretical (left) and experimental (right) NRIXS spectra with the momentum transfer directed along the ΓK direction using several values of q .

symmetry line Γ -M but not along the line Γ -K. The anisotropic splitting is an effect of the anisotropic dispersion of the π -bands. We have detected an anisotropy in the electron-hole interaction for momentum transfer parallel/perpendicular to the layers. For q_{\parallel} , the electron and the hole tend to form a strongly bound quasi-two dimensional compound while for q_{\perp} electron and hole tend to be localized on different layers and form a weakly bound three-dimensional compound. This anisotropy explains the 0.7 eV difference in the blueshift that must be added to the RPA spectra (which neglect the effect of electron-correlation) in order to match the experimental data.

This work was supported by the Academy of Finland (1127462/110571), Spanish MEC (FIS2007-65702-C02-01), "Grupos Consolidados UPV/EHU del Gobierno Vasco" (IT-319-07), the European Community through e-I3 ETSF project (GA. 211956). JAS benefited from the CMS Network RIXS collaboration supported by the U.S. DoE (grant DE-FG02-08ER46540). AR benefit from fundamental discussions and collaboration with Prof. T. Pichler. Computing time was provided by the "Red Espanola de Supercomputaci3n" and IDRIS (Proj. No. 091827).

-
- [1] K. Watanabe, T. Taniguchi, and H. Kanda, *Nat. Mat.* **3**, 404 (2004).
 - [2] X. Blase, A. Rubio, S. G. Louie, and M. L. Cohen, *Phys. Rev. B* **51**, 6868 (1995).
 - [3] B. Arnaud, S. Lebégue, P. Rabiller, and M. Alouani, *Phys. Rev. Lett.* **96**, 026402 (2006).
 - [4] L. Wirtz, A. Marini, and A. Rubio, *Phys. Rev. Lett.* **96**, 126104 (2006).
 - [5] A. Marini, *Phys. Rev. Lett.* **101**, 106405 (2008).
 - [6] L. Wirtz, A. Marini, M. Grüning, C. Attaccalite, G. Kresse, and A. Rubio, *Phys. Rev. Lett.* **100**, 189701 (2008).
 - [7] B. Arnaud, S. Lebégue, P. Rabiller, and M. Alouani, *Phys. Rev. Lett.* **100**, 189702 (2008).
 - [8] K. Watanabe and T. Taniguchi, *Phys. Rev. B* **79**, 193104 (2009).
 - [9] P. Jaffrennou, J. Barjon, J.-S. Lauret, B. Attal-Trétout, F. Ducastelle, and A. Loiseau, *J. Appl. Phys.* **102**, 116102 (2008).
 - [10] L. Museur, E. Feldbach, and A. Kanaev, *Phys. Rev. B* **78**, 155204 (2008).
 - [11] K. Watanabe, T. Taniguchi, T. Kuroda, and H. Kanda, *Applied Physics Letters* **89**, 141902 (pages 3) (2006), URL <http://link.aip.org/link/?APL/89/141902/1>.
 - [12] L. Liu, Y. P. Feng, and Z. X. Shen, *Phys. Rev. B* **68**, 104102 (2003).
 - [13] N. Ooi, A. Rairkar, L. Lindsley, and J. B. Adams, *J. Phys.: Condens. Matter* **18**, 97 (2006).
 - [14] G. Satta, G. Cappellini, V. Olevano, and L. Reining, *Phys. Rev. B* **70**, 195212 (2004).
 - [15] W. A. Caliebe, J. A. Soininen, E. L. Shirley, C.-C. Kao, and K. Hämäläinen, *Phys. Rev. Lett.* **84**, 3907 (2000).
 - [16] G. G. Fuentes, E. Borowiak-Palen, T. Pichler, X. Liu, A. Graff, G. Behr, R. J. Kalenczuk, M. Knupfer, and J. Fink, *Phys. Rev. B* **67**, 035429 (2003).
 - [17] P. Abbamonte, T. Graber, J. P. Reed, S. Smadici, C. L. Yeh, A. Shukla, J. P. Rueff, and W. Ku, *Proc. Nat. Acad. Sci.* **105**, 12159 (2008).
 - [18] J. A. Soininen and E. L. Shirley, *Phys. Rev. B* **61**, 16423 (2000).
 - [19] S. Galambosi, J. A. Soininen, A. Mattila, S. Huotari, S. Manninen, G. Vankó, N. D. Zhigadlo, J. Karpinski, and K. Hämäläinen, *Phys. Rev. B* **71**, 060504(R) (2005).
 - [20] Y. Q. Cai, P. C. Chow, O. D. Restrepo, Y. Takano, K. Togano, H. Kito, H. Ishii, C. C. Chen, K. S. Liang, C. T. Chen, et al., *Phys. Rev. Lett.* **97**, 176402 (2006).
 - [21] C. Tarrio and S. E. Schnatterly, *Phys. Rev. B* **40**, 7852 (1989).

- [22] S. Huotari, G. Vankó, F. Albergamo, C. Ponchut, H. Graafsma, C. Henriquet, R. Verbeni, and G. Monaco, *J. Synchrotron Rad.* **12**, 467 (2005).
- [23] R. Verbeni, T. Pylkkänen, S. Huotari, L. Simonelli, G. Vankó, K. Martel, C. Henriquet, and G. Monaco, *J. Synchrotron Rad.* **16**, 469 (2009).
- [24] K. Hämäläinen, S. Manninen, C.-C. Kao, W. Caliebe, J. B. Hastings, A. Bansil, S. Kaprzyk, and P. M. Platzman, *Phys. Rev. B* **54**, 5453 (1996).
- [25] DFT calculations have been performed with **ABINIT**[32]. The wave-functions are expanded in plane waves with an energy cutoff of 25 Hartree. The 1s electrons are included in the Troullier-Martins pseudopotentials. Lattice parameters $a = 2.504 \text{ \AA}$ and $c = 6.660 \text{ \AA}$ were used [33].
- [26] S. L. Adler, *Phys. Rev.* **126**, 413 (1962).
- [27] The matrix $\epsilon_{\mathbf{G},\mathbf{G}'}$ comprises a total of 80 \mathbf{G} vectors in our calculations. The 1st BZ is sampled with a $60 \times 60 \times 4$ k -point grid for the calculations with q parallel to the hexagonal plane and with a $30 \times 30 \times 12$ grid for calculations with q perpendicular to it. We have included 8 occupied and 52 unoccupied bands, up to an energy of 70 eV above the valence band maximum. Calculations have been performed with **Yambo** [34].
- [28] H.-C. Weissker, J. Serrano, S. Huotari, F. Bruneval, F. Sottile, G. Monaco, M. Krisch, V. Olevano, and L. Reining, *Phys. Rev. Lett.* **97**, 237602 (2006).
- [29] G. Onida, L. Reining, and A. Rubio, *Rev. Mod. Phys.* **74**, 601 (2002).
- [30] L. X. Benedict and E. L. Shirley, *Phys. Rev. B* **59**, 5441 (1999).
- [31] A k -space grid of $24 \times 24 \times 12$, a \mathbf{G} -grid of $5 \times 5 \times 5$ and 32 unoccupied bands were used in these calculations. Finally a broadening of 0.4 eV was applied for the comparison.
- [32] X. Gonze, J.-M. Beuken, R. Caracas, F. Detraux, M. Fuchs, G.-M. Rignanese, L. Sindic, M. Verstraete, G. Zerah, F. Jollet, et al., *Comp. Mat. Sci.* **25**, 478 (2002).
- [33] V. L. Solozhenko, G. Will, and F. Elf, *Solid State Commun.* **96**, 1 (1995).
- [34] A. Marini, C. Hogan, M. Grüning, and D. Varsano, *Comp. Phys. Comm.* **180**, 1392 (2009).